





Cite this: *Nanoscale*, 2023, **15**, 17583

Light-sensitive monolayer-thick nanocrystal skins of face-down self-oriented colloidal quantum wells†

Taylan Bozkaya,^a Furkan Isik,^a  Iklm Bozkaya,^a Savas Delikanli,^{a,b} Emre Unal^a and Hilmi Volkan Demir  ^{*a,b}

Colloidal quantum wells (CQWs), a quasi-two-dimensional, atomically-flat sub-family of semiconductor nanocrystals, are well suited to produce excellent devices for photosensing applications thanks to their extraordinarily large absorption cross-sections. In this work, we propose and demonstrate a new class of light-sensitive nanocrystal skins (LS-NS) that employ a monolayer of face-down orientation-controlled self-assembled CQWs as the active absorbing layer in the UV-visible range. This CQW LS-NS platform enables non-conventional photosensing operation that relies on the strong optical absorption of the monolayered assembly of CQWs and the subsequent photogenerated potential build-up across the device, allowing for self-powered operation. Here such self-oriented CQWs reduce the surface roughness in their monolayer-thick film, essential to high device performance. Owing to their ease of fabrication and low cost, these devices hold great promise for large-scale use in semi-transparent photosensing surfaces.

Received 13th August 2023,
Accepted 13th October 2023

DOI: 10.1039/d3nr04065h

rsc.li/nanoscale

Introduction

Colloidal quantum wells (CQWs), belonging to the quasi-two-dimensional sub-family of semiconductor nanocrystals, provide superior optical properties.^{1–8,23,24} CQWs possess a well-defined vertical thickness owing to their atomically-flat structure across the entire lateral extension.^{9–13,15} With a vertical thickness of few monolayers, such a quasi-two-dimensional quantum structure leads to remarkably large absorption cross-sections. Their customizable absorption spectrum further provides a degree of freedom to tune their absorption-based photosensing functionality and performance in operation. Synthesized using wet chemistry, these CQWs are solution-processable to fabricate their devices, which significantly reduces their processing costs.

Recent research on CQWs has showed ways to self-assemble CQWs of a specific orientation.^{14,26} Since a self-assembly process can be employed to obtain only a single monolayer of CQWs in one targeted orientation in the film, such an orien-

tation-dictating approach provides us with the ability to achieve excellent control also over the film thickness while keeping the film's roughness to a minimum to fabricate highly reproducible, precisely-constructed devices.¹⁴ As long as the sub-phase required for such a self-assembly method is chosen to be compatible with the substrate (and the device layers if any) in use, this approach is essentially applicable to any solution-based processing. Considering the capability to self-assemble a monolayer film of CQWs, combined with their favorable optical properties, CQWs offer great promise for absorptive devices such as photodetectors.

Based on optical absorption, light-sensitive nanocrystal skins (LS-NS) are constructed in a non-conventional photosensitive device architecture that relies on the principle of photogenerated voltage build-up, demonstrated to be a versatile and efficient device platform.¹⁶ The concept of LS-NS can be applied to different device architectures making use of tandem²² and exciton funneling¹⁹ configurations as well. Furthermore, this device structure has also been demonstrated on various substrates, including semi-transparent and flexible substrates.^{16–22} Finally, since the photogenerated voltage build-up allows for a self-powered operation mode, this device platform does not require any external power supply, making it highly attractive from the external power consumption point of view.¹⁶

In this work, to utilize the attractive properties of CQWs and leverage on the orientation control in the self-assembly of CQW, we propose and demonstrate the LS-NS device platform of orientation controlled self-assembled 4.5 monolayers (ML)

^aDepartment of Electrical and Electronics Engineering, Department of Physics, UNAM– Institute of Materials Science and Nanotechnology, and The National Nanotechnology Research Center, Bilkent University, Ankara 06800, Turkey. E-mail: volkan@bilkent.edu.tr

^bLuminous! Center of Excellence for Semiconductor Lighting and Displays, School of Electrical and Electronic Engineering, School of Physical and Mathematical Sciences, School of Materials Science and Engineering, Nanyang Technological University, 50 Nanyang Avenue, Singapore 639798, Singapore. E-mail: hvdemir@ntu.edu.sg

† Electronic supplementary information (ESI) available. See DOI: <https://doi.org/10.1039/d3nr04065h>

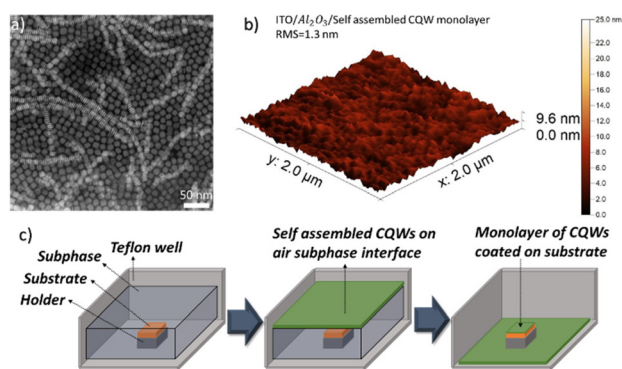


Fig. 1 (a) Transmission electron microscopy (TEM) image of 4.5 ML CdSe CQWs (b) atomic force microscopy (AFM) of self-assembled 4.5 ML CdSe CQW film on top of ITO substrate coated with Al₂O₃ with thermal atomic layer deposition (ALD) method with film roughness of root mean square (RMS) 1.3 nm. (c) Process flow of oriented CQW self-assembly.

CdSe CQWs in the face-down orientation as the active layer, operating in the UV-visible range (Fig. 1). Although a variety of LS-NS devices have been previously demonstrated using colloidal quantum dots,^{16–22} this is the first account of a LS-NS device based on the colloidal quantum wells. This work is also first proof-of-concept demonstration of the use of face-down orientation-controlled CQWs in such an absorptive device.

Results and discussion

We synthesized 4.5 ML thick CdSe CQWs (according to the recipe given in the ESI, S1†). Transmission electron microscopy of the as-synthesized CQWs is shown in Fig. 1a. These CQWs provide an optical absorption cross-section of $9 \times 10^{-14} \text{ cm}^2$.²⁵ We conducted the self-assembly process of these CQWs as explained in a previous study.¹⁴ Device fabrication using the CQWs was carried out according to a previous report.¹⁶ Here we utilized Al₂O₃ instead of HfO₂ as the oxide layer as the current-blocking layer and shortened the processing time, different than the previous work. In the fabrication, we first coated ITO-precoated substrates having an ITO thickness of around 100 nm and sheet resistance of 2.5 ohm/sq with a 100 nm thick Al₂O₃ film at 300 °C by atomic layer deposition (ALD). After this deposition, we proceeded with the self-assembly of CQWs on top of the dielectric layer. Finally, we coated a 40 nm thick Al on top of the CQW layer to make the final metal contact (Al) on the top by using thermal evaporation.

The self-assembly is a critical aspect of this study, considering the significant reduction of the surface roughness (Fig. 1b) along with the robust control of the CQW film's thickness with its conformality of the layer. In the self-assembly process, we fixed the substrate on top of a holder using double-sided tape, placed it into a Teflon Petri dish, and slowly poured the subphase inside the dish. Here it is crucial not to leave any air

bubbles inside the subphase, which can surface later and distort the self-assembled film at the subphase interface. Also, the subphase's depth should be reasonable; if it is too shallow, the substrate and holder start to interfere with the surface interactions, and if subphase level is too high, interactions increase with the edges of the well, making it challenging to preserve conformality of the film during the draining process (Fig. 1c). The height of the subphase above the substrate is 3–4 mm in this work. Subsequently we carefully dropped the CQW solution on top of the subphase by using a micropipette at a predetermined amount. We waited until the end of the process of self-assembly while the solvent of CQWs evaporated slowly. After evaporation, with the help of an injector, we drained the entire subphase from the bottom of the container. Finally, we placed the substrate under vacuum until residual subphase further evaporated. At the end of this step, we have the monolayer CQW film successfully placed on top of the substrate. The surface roughness of the CQWs was found to be 1.3 nm thanks to their self-assembly on top of the ITO/Al₂O₃, which also has reduced RMS roughness from 3.5 nm (for ITO substrate (S2a†)) to 1.8 nm (S2b†).

Fig. 2a shows the scanning electron microscopy image of the monolayer face-down self-assembled 4.5 ML CdSe CQW film used in the device architecture (Fig. 2b). Owing to the device architecture of this LS-NS platform (Fig. 2c), charge carriers cannot pass through the device because of the current-blocking dielectric film of Al₂O₃. Hence, when not connected, the device is in open circuit and acts like a parallel-plate capacitor to be charged upon optical excitation, starting from uncharged state. Under optical illumination, electron and hole

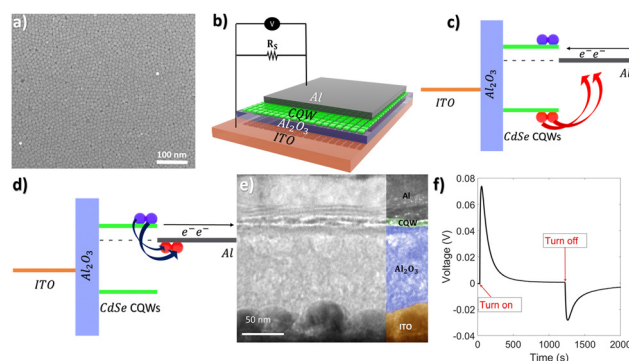


Fig. 2 (a) Scanning electron microscopy (SEM) image of monolayer face-down self-assembled 4.5 ML CdSe CQW film. CQWs (b) Illustrative schematic of the CQW LS-NS device, which shows each layer of the device, additionally depicting the external circuitry that consisting of contacts, the external circuit, connected shunt resistance, and voltmeter, (c) simplified energy band diagram showing the carrier transfer throughout the excitation phase of photovoltage build-up, (d) simplified energy band diagram carrier transfer of the photovoltage build-up throughout the phase which the excitation source is turned off, (e) transmission electron microscopy of the cross section of the LS-NS device, (f) voltage-time trace in standard device operation mode. Here the photovoltage build-up is observed with "turn on" marking the point in time at which the excitation source is turned on. "Turn off" marks the point at which the excitation source is turned off.

pairs are photogenerated in the self-assembled monolayer of CQWs and dissociated at the CQW-Al interface. Holes are then transferred to and accumulated on the Al side, whereas electrons stay on the CQW side due to the workfunction of Al and the valence and conduction bands of the CQW layer. Therefore, in the LS-NS device, positive and negative charge accumulations are internally on the opposite sides (in the Al and CQW layers, respectively), as sketched in Fig. 2c. Those dissociated electron-hole pairs at the CQW-Al interface are held across the device capacitively as the stored charges.

The photovoltage build-up highly depends on the capacitive charging of the metal-semiconductor contact as the device itself is in a transient state. This LS-NS device can be considered as an RC circuit element. When connected externally through a shunt resistor of a predetermined value, the LS-NS device is able to discharge the photovoltage at a desired rate (Fig. 2b). As can be seen in Fig. 2c, externally circulating electrons neutralize the charged device. As a result, one observes a transient voltage response (voltage vs. time) as presented in Fig. 2f (during the excitation phase), which grows exponentially due to the continuous excitation and simultaneously

decays due to the RC decay. After the excitation source is turned off, the photogenerated electron-hole pairs are no longer separated; instead, electrons on the CQW side start recombining on the aluminum side, as illustrated in Fig. 2d. This situation leaves externally neutralizing electrons as additional charges on the aluminum side (leaving behind holes alone as the positive charges on the ITO side). This leads to an inverse voltage build-up (Fig. 2f) with a magnitude correlated to the intensity of optical illumination and the exposure time, which can be interpreted as a memory effect.¹⁶

We use eqn (1) to predict the photovoltage build-up over time. Here, the term A represents the upper capped value of the build-up voltage, which purely depends on the number of photogenerated excitons available for separation. The first term of eqn (1) is an inverse exponential process in time. The second term on the right-hand side of eqn (1) is the RC decay term of a parallel plate capacitor. This represents the discharging process of the device *via* the external circuitry through the parallel shunt resistor connected to the device. These first and second terms of eqn (1) are multiplied because they are simultaneous processes competing each other. In eqn (1), R_S denotes the resistance of the externally connected shunt resistor. C stands for the effective capacitance of the device between the ITO and aluminum contacts. Finally, G stands for the generation rate. Here note that G and A are both empirically measured.

$$V(t) = A(1 - e^{-G(t-t_0)}) \times e^{-\frac{1}{R_S C}(t-t_0)} \quad (1)$$

Next we investigate the relation of the excitation power to the device operation by systematically varying it. We observe here with the self-assembled CQW monolayer as the device's active film that the RC decay mechanism is profoundly affected in the LS-NS devices (Fig. 3). We find that the RC decay time constant of the device is decreasing as we repeat the turn-on and turn-off cycles consecutively. This decrease can be attributed to the change in the device's capacitance, and it is considered to be a consequence of the change in the effective dielectric constant of the CQW layer.¹⁶ The overall capacitance is decreased throughout the device for consecutive measurements (repetition numbers 2,3 and 4) (Table 1). As the excitation power changes, we observed a slight variation in the RC decay time, a critical parameter for calculating the capacitance and effective dielectric constant. Here we obtain significantly larger capacitance for CQW LS-NS devices around 55 nF for each power setting, whereas for the colloidal quantum dot (CQD) based LS-NS devices this value is averaged at around 38

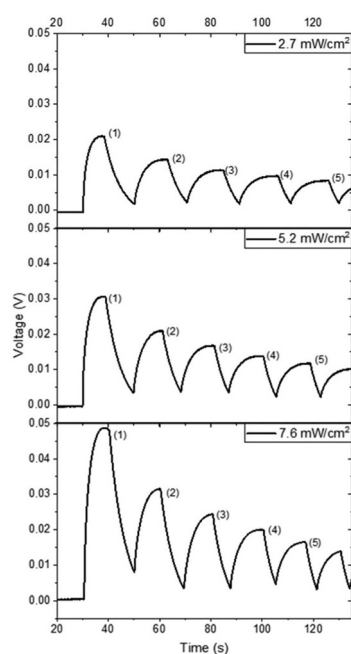


Fig. 3 Photovoltage build-up and RC decay of LS-NS device, upon turning on and off the excitation source (for 5 times as displayed) at different excitation power levels at 405 nm: 2.7, 5.2, and 7.6 mW cm⁻².

Table 1 RC decay times calculated at the turn-off points in Fig. 3 at the corresponding excitation power level

	2.7 mW cm ⁻²			5.2 mW cm ⁻²			7.6 mW cm ⁻²		
	RC (s)	C (nF)	ϵ_{CdSe}	RC (s)	C (nF)	ϵ_{CdSe}	RC (s)	C (nF)	ϵ_{CdSe}
1	5.42	54.2	0.26	5.51	55.1	0.28	5.48	54.8	0.27
2	4.57	45.7	0.23	4.54	45.4	0.23	4.58	45.8	0.23
3	3.97	39.7	0.20	3.91	39.1	0.20	3.92	39.2	0.20
4	3.46	34.6	0.18	3.31	33.1	0.17	3.47	34.7	0.18
5	3.07	30.7	0.16	3.00	30.0	0.15	3.08	30.8	0.16

nF for each power setting. More significantly, if we look at the values of capacitance per unit area, we find 24.44 nF cm^{-2} for CQW LS-NS (2.25 cm^2 of active area) and 0.79 nF cm^{-2} for CQD LS-NS (48 cm^2 of active area).¹⁶

Also, we study the excitation power dependence of the photovoltage build-up (Fig. 4a). As the excitation power increases, we observe a decrease in the sensitivity (Fig. 4b) due to the saturation of the active layer. Furthermore, we conducted spectral sensitivity measurements to understand the spectral response of the CQW LS-NS device. For this characterization, using a monochromator, we scanned the optical excitation spectrum from 450 to 550 nm. We recorded incident optical power while carrying out the photovoltage build-up measurements at each wavelength. Next, we calculated the peak sensitivity for each measurement (Fig. 4c). On the measured spectral sensitivity curve, we observe the first (heavy-hole) and second (light-hole) excitonic absorption peaks of the CQWs as this curve mimics the spectral profile of the optical absorbance of CQWs. This similarity provides another opportunity for the device to utilize; with the right design and filtering, one can simultaneously utilize the same active material (CQWs) as an active layer in multiple different spectral windows. Finally, we observe a cut-off wavelength near 512 nm for these CQWs. Similarly, we do not read any signal from our device beyond this spectral point. Thus, the sensitivity is practically zero above the cut-off wavelength of 512 nm.

Another critical aspect is that optical absorption levels out in the spectral range shorter than 375 nm on the absorbance spectrum, while what we observe in the sensitivity spectrum is

quite the opposite since the spectral sensitivity keeps growing. Because each absorbed photon with a higher photon energy than the band gap creates an electron-hole pair independent of their energy. However, excess energy is also transferred into the photogenerated pair; conventionally, this energy is thermally lost as the electron and hole relax towards the band edge. However, in the device's operation, we utilize the hopping of the charges across the aluminum interface and the CQW layer, for which we reckon excess energy becomes helpful as hot carrier for this process. Effective separation occurs at the interface, and effective separation at the contact leads to a larger voltage build-up, hence the increased sensitivity.

Furthermore, we investigate the photocharging effect. We found out that, as the time of illumination increases, we observe a larger negative peak once the excitation source is turned off (Fig. 4d) (when we use a constant excitation power during the excitation time). This effect is directly proportional to the total number of collected electrons from the external circuitry during the excitation phase. This phenomenon is explained as a memory effect.¹⁶ If we compare our CQW LS-NS device with its CQD counterpart in terms of the photocharging capability, we can see that CQW-based devices have a larger photocharging capability. The CQD LS-NS reaches a maximum negative peak of 20 mV after 30 min of illumination, however our CQW LS-NS reaches the similar negative peak of 20 mV only after 5 min of illumination and later a maximum of 30 mV after 35 min of illumination.¹⁶

Our final characterization is the photovoltage build-up of the CQW LS-NS device with different values of shunt resistance

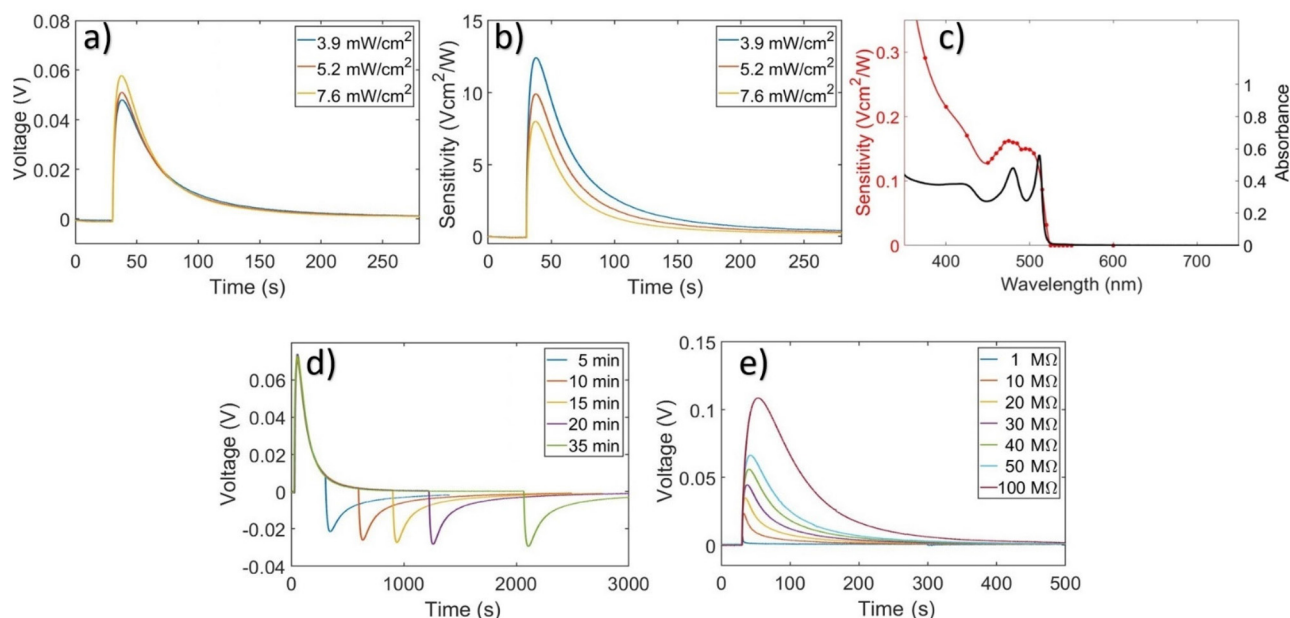


Fig. 4 (a) Photovoltage build-up measurements at different excitation power levels at 405 nm. (b) Photosensitivity calculated using the photovoltage build-up curve divided by the excitation power. (c) Spectral absorbance plotted together with spectral photosensitivity. (d) Photocharging effect shown through photovoltage build-up measurements by turning the excitation source off at different time marks at the same excitation power at 405 nm. (e) Photovoltage build-up utilizing 405 nm excitation source at the same power while parallel shunt resistors being connected with varied resistance.

(Fig. 4e). The signal amplitude grows as the shunt resistance increases. This trend of increasing voltage complies with the predictions of eqn (1). Since the generation parameter is constant (the first term of eqn (1)), the RC time constant that is growing larger with increasing the shunt resistance exposes the device to a slower decay. As a result, we obtain an increasing trend in the photovoltage build-up at the cost of a slower response.

Conclusions

In conclusion, we have developed and demonstrated an LS-NS device employing the face-down oriented self-assembled monolayer of all solution-processed CQWs as the active layer of the device platform. We reduced the surface roughness of the CQWs to 1.3 nm *via* their self-assembly. These devices are highly efficient in terms of power consumption during operation since they work on the principle of their own photogenerated voltage build-up. This operation principle requires neither external biasing nor externally applied current running through the device. We found that spectral sensitivity mimics the absorption spectra of CQWs at the excitonic peaks as expected. However, at the lower end of the spectrum, we found a sharp rise of sensitivity different from the absorption spectra of CQWs. This difference is attributed to the more effective separation of excitons at the CQW-Al interface due to the excess energy provided by the higher-energy photons. The effect of shunt resistance is vital to a balanced operation; as its value increases, the voltage build-up increases at the cost of a slower response, which also complies with the computational predictions we made. For future work, we intend to investigate the impact of the orientation of the CQW active layer since we can change the orientation of such a self-assembled monolayer CQW film to edge-up.

Author contributions

The authors confirm contribution to the paper as follows: device conception: Hilmi Volkan Demir; device design: Taylan Bozkaya and Hilmi Volkan Demir; device fabrication and characterization: Taylan Bozkaya; synthesis of colloidal materials: Furkan Isik and Iklim Bozkaya; process of self-assembly: Taylan Bozkaya, Iklim Bozkaya, and Furkan Isik; analyses and interpretation of results: Taylan Bozkaya, Furkan Isik, Savas Delikanli, Emre Unal, and Hilmi Volkan Demir; draft manuscript preparation: Taylan Bozkaya, Furkan Isik, Savas Delikanli, Emre Unal, and Hilmi Volkan Demir. All authors reviewed the results and approved the final version of the manuscript.

Conflicts of interest

There are no conflicts to declare.

Acknowledgements

The authors gratefully acknowledge the financial support in part from the Singapore Agency for Science, Technology and Research (A*STAR) MTC program under grant number M21J9b0085, Ministry of Education, Singapore, under its Academic Research Fund Tier 1 (MOE-RG62/20), and in part from TUBITAK 119N343, 121C266, 121N395, 120N076 and 20AG001. H.V.D. also acknowledges support from TUBA and TUBITAK 2247-A National Leader Researchers Program (121C266).

References

- H. Eisler, V. C. Sundar, M. G. Bawendi, M. Walsh, H. I. Smith and V. I. Klimov, Color-selective semiconductor nanocrystal laser, *Appl. Phys. Lett.*, 2002, **80**(24), 4614–4616.
- R. D. Schaller, M. A. Petruska and V. I. Klimov, Tunable Near-Infrared optical gain and amplified spontaneous emission using PBSE nanocrystals, *J. Phys. Chem. B*, 2003, **107**(50), 13765–13768.
- L. Manna, D. J. Milliron, A. Meisel, E. C. Scher and A. P. Alivisatos, Controlled growth of tetrapod-branched inorganic nanocrystals, *Nat. Mater.*, 2003, **2**(6), 382–385.
- J. Joo, J. S. Son, S. G. Kwon, J. H. Yu and T. Hyeon, Low-Temperature Solution-Phase synthesis of quantum well structured CDSE nanoribbons, *J. Am. Chem. Soc.*, 2006, **128**(17), 5632–5633.
- J. M. Pietryga, R. D. Schaller, D. J. Werder, M. H. Stewart, V. I. Klimov and J. A. Hollingsworth, Pushing the band gap envelope: Mid-Infrared Emitting Colloidal PBSE Quantum dots, *J. Am. Chem. Soc.*, 2004, **126**(38), 11752–11753.
- C. B. Murray, C. R. Kagan and M. G. Bawendi, Synthesis and characterization of monodisperse nanocrystals and Close-Packed nanocrystal assemblies, *Annu. Rev. Mater. Sci.*, 2000, **30**(1), 545–610.
- S. Kim, B. Fisher, H. Eisler and M. G. Bawendi, Type-II quantum dots: CDTE/CDSE(Core/Shell) and CDSE/ZNTE (Core/Shell) heterostructures, *J. Am. Chem. Soc.*, 2003, **125**(38), 11466–11467.
- M. A. Hines and P. Guyot-Sionnest, Synthesis and Characterization of Strongly Luminescing ZnS-Capped CdSe Nanocrystals, *J. Phys. Chem.*, 1996, **100**, 468–471.
- Y. S. Park, J. Roh, B. T. Diroll, R. D. Schaller and V. I. Klimov, Colloidal quantum dot lasers, *Nat. Rev. Mater.*, 2021, **6**(5), 382–401.
- F. Garcia-Santamaria, Y. Chen, J. Vela, R. D. Schaller, J. A. Hollingsworth and V. I. Klimov, Suppressed auger recombination in “Giant” nanocrystals boosts optical gain performance, *Nano Lett.*, 2009, **9**(10), 3482–3488.
- L. T. Kunneman, M. Tessier, H. Heuclin, B. Dubertret, Y. V. Aulin, F. C. Grozema, J. M. Schins and L. D. A. Siebbeles, Bimolecular auger recombination of Electron–Hole pairs in Two-Dimensional CDSE and CDSE/

- CDZNS Core/Shell nanoplatelets, *J. Phys. Chem. Lett.*, 2013, **4**(21), 3574–3578.
- 12 S. Delikanli, O. Erdem, F. Isik, H. D. Baruj, F. Shabani, H. B. Yagci, E. G. Durmusoglu and H. V. Demir, Ultrahigh Green and Red Optical Gain Cross Sections from Solutions of Colloidal Quantum Well Heterostructures, *J. Phys. Chem. Lett.*, 2021, **12**(9), 2177–2182.
- 13 C. She, I. Fedin, D. S. Dolzhenkov, A. Demortière, R. D. Schaller, M. Pelton and D. V. Talapin, Low-Threshold stimulated emission using colloidal quantum wells, *Nano Lett.*, 2014, **14**(5), 2772–2777.
- 14 O. Erdem, K. Gungor, B. Guzelurk, I. Tanriover, M. Sak, M. Olutas, D. Dede, Y. Kelestemur and H. V. Demir, Orientation-Controlled nonradiative energy transfer to colloidal nanoplatelets: Engineering Dipole Orientation Factor, *Nano Lett.*, 2019, **19**(7), 4297–4305.
- 15 A. W. Achtstein, A. Antanovich, A. Prudnikau, R. Scott, U. Woggon and M. Artemyev, Linear absorption in CDSE nanoplates: thickness and lateral size dependency of the intrinsic absorption, *J. Phys. Chem. C*, 2015, **119**(34), 20156–20161.
- 16 S. Akhavan, B. Guzelurk, V. Sharma and H. Demir, Large-area semi-transparent light-sensitive nanocrystal skins, *Opt. Express*, 2012, **20**, 25255–25266.
- 17 S. Akhavan, A. Yeltik and H. V. Demir, Photosensitivity Enhancement with TiO₂ in Semitransparent Light-Sensitive Skins of Nanocrystal Monolayers, *ACS Appl. Mater. Interfaces*, 2014, **6**(12), 9023–9028.
- 18 S. Akhavan, K. Gungor, E. Mutlugun and H. V. Demir, Plasmonic light-sensitive skins of nanocrystal monolayers, *Nanotechnology*, 2013, **24**(15), 155201.
- 19 S. Akhavan, A. Cihan, B. Bozok and H. V. Demir, Nanocrystal Skins with Exciton Funneling for Photosensing, *Small*, 2014, **10**(12), 2470–2475.
- 20 S. Akhavan, M. Z. Akgul, P. L. Hernandez-Martinez and H. V. Demir, Plasmon-Enhanced energy transfer in photosensitive nanocrystal device, *ACS Nano*, 2017, **11**(6), 5430–5439.
- 21 S. Akhavan, A. Cihan, A. Yeltik, B. Bozok, V. Lesnyak, N. Gaponik, A. Eychmüller and H. V. Demir, Multiexciton generation assisted highly photosensitive CdHgTe nanocrystal skins, *Nano Energy*, 2016, 324–331.
- 22 S. Akhavan, C. Uran, B. Bozok, K. Gungor, Y. Kelestemur, V. Lesnyak, N. Gaponik, A. Eychmüller and H. V. Demir, Flexible and fragmentable tandem photosensitive nanocrystal skins, *Nanoscale*, 2016, **8**(8), 4495–4503.
- 23 G. Bertrand, A. Polovitsyn, S. Christodoulou, A. H. Khan and I. Moreels, Shape control of zincblende CdSe nanoplatelets, *Chem. Commun.*, 2016, **52**(80), 11975–11978.
- 24 M. Olutas, B. Guzelurk, Y. Kelestemur, A. Yeltik, S. Delikanli and H. V. Demir, Lateral Size-Dependent spontaneous and Stimulated emission properties in colloidal CDSE nanoplatelets, *ACS Nano*, 2015, **9**(5), 5041–5050.
- 25 A. Yeltik, S. Delikanli, M. Olutas, Y. Kelestemur, B. Guzelurk and H. V. Demir, Experimental Determination of the Absorption Cross-Section and Molar Extinction Coefficient of Colloidal CdSe Nanoplatelets, *J. Phys. Chem. C*, 2015, **119**(47), 26768–26775.
- 26 O. Erdem, S. Foroutan, N. Gheshlaghi, B. Guzelurk, Y. Altintas and H. V. Demir, Thickness-Tunable Self-Assembled Colloidal Nanoplatelet Films Enable Ultrathin Optical Gain Media, *Nano Lett.*, 2020, **20**(9), 6459–6465.